Predicting surface free energies with interatomic potentials and electron counting

2005 J. Phys.: Condens. Matter 17 6123

(http://iopscience.iop.org/0953-8984/17/39/002)

INSTITUTE OF PHYSICS PUBLISHING JOURNAL OF PHYSICS: CONDENSED MATTER

J. Phys.: Condens. Matter **17** (2005) 6123–6137 doi:10.1088/0953-8984/17/39/002

Predicting surface free energies with interatomic potentials and electron counting

D A Murdick[1,3], X W Zhou[1], H N G Wadley[1] and D Nguyen-Manh[2]

[1] School of Engineering and Applied Science, University of Virginia, Charlottesville, VA 22904, USA
[2] UKAEA Culham Division, Culham Science Centre, Abingdon OX14 3DB, UK

E-mail: murdick@mailaps.org

Received 18 July 2005
Published 16 September 2005
Online at stacks.iop.org/JPhysCM/17/6123

Abstract

Current interatomic potentials for compound semiconductors, such as GaAs, fail to correctly predict the *ab initio* calculated and experimentally observed surface reconstructions. These potentials do not address the electron occupancies of dangling bonds associated with surface atoms and their well established role in the formation of low-energy surfaces. The electron counting rule helps account for the electron distribution among covalent and dangling bonds, which, when applied to GaAs surfaces, requires the arsenic dangling bonds to be fully occupied and the gallium dangling bonds to be empty. A simple method for linking this electron counting constraint with interatomic potentials is proposed and used to investigate energetics of the atomic scale structures of the GaAs(001) surface using molecular statics methods.

1. Introduction

In the modelling of the vapour phase epitaxial growth of semiconducting materials, it is important to correctly predict surface structure and energy. This requires computationally efficient models that accurately predict relevant energies and structures. *Ab initio* methods can provide the needed level of energy precision [1, 2], but the calculations are too slow for directly studying thin film growth. Numerically efficient Monte Carlo methods using precomputed energy barriers and atomic transition paths are able to simulate the assembly of a large number of atoms but ignore the important effects of interatomic forces and local stresses upon the assembly process [3, 4]. The use of classical interatomic potentials in molecular dynamics simulations provides a practical compromise between efficiency and accuracy, provided high-fidelity potential energy functions are available [5].

[3] Author to whom any correspondence should be addressed.

An evaluation of many of the available GaAs potentials has recently been conducted [6]. The Albe *et al* [7] parametrization of Tersoff's potential (TR-ANNK) [8, 9] and two parametrizations of the Stillinger–Weber [10] potential format by Wang and Stroud (SW-WS) [11] and by Angelo and Mills [12] and Grein *et al* (SW-AMG+) [13] were found to be best suited for molecular dynamics simulations of GaAs surfaces. However, all three potentials were shown to be unable to predict any of the complex surface reconstruction structures that have been observed for the GaAs(001) surface [14–17]. In fact, no potential reported to date has been shown to correctly predict the experimentally observed and density functional theory (DFT) calculated (001) surface reconstructions of GaAs.

The free surface of bulk-terminated polar semiconductors, such as GaAs, is driven to relax and reconstruct its surface geometry in order to reduce the number of electrons in high-energy sp^3 dangling bond hybrid orbitals. For GaAs(001), this results in surface dimerization of arsenic and gallium atom pairs and electron transfer from high- to low-energy dangling bonds [18]. The electron counting (EC) rule [19, 20], has provided a simple means for the identification of surface structures that minimize the occupancy of high-energy dangling bonds.

Here a method for linking the notion of electron counting with classical potentials is developed, and its utility for predicting the surface reconstructions of GaAs(001) is explored for three potential parametrizations. Minimum energy GaAs(001) surface geometries are calculated for several reconstructions over a wide range of surface compositions using molecular statics methods. The addition of an EC rule motivated energy term to the potentials is shown to improve the ability of the modified potentials to predict GaAs(001) surface structures.

2. (001) surfaces

2.1. Surface reconstructions

Approximately 100 surface structures have been proposed for the GaAs(001) surface and about a dozen surface reconstructions have been experimentally observed [21]. Each of the observed structures has been shown to be dependent upon the vapour and surface composition and surface temperature. Several of the GaAs(001) surfaces most germane to subsequent discussions are shown in figure 1. Not all of the (001) surface reconstructions shown have been experimentally validated; the selections were used to highlight the wide range of possible surface configurations that a GaAs(001) surface can assume.

The bulk-terminated (1×1) (001) surface, figure 1(a), is the simplest surface structure to consider. It is created by cleaving the Ga–As bonds of a zinc blende (zb) GaAs crystal to expose a layer of either arsenic or gallium atoms. The as-cleaved arsenic-terminated surface is shown in figure 1(a). The gallium-terminated surface is essentially the same as the arsenic termination but with the atom type swapped. This (1×1) surface has been experimentally reported using *in situ* reflection high-energy electron diffraction (RHEED) only during low-temperature (523 K) molecular beam epitaxial growth [22].

The arsenic-rich (1×2), figure 1(b), and gallium-rich (2×1), figure 1(c), surfaces have rows of either arsenic or gallium dimers. This dimerization reduces the number of dangling bonds and has a lower energy than the bulk-terminated structures. While these configurations have been experimentally observed on Si(001) surfaces [23, 24], there are no reports of their presence on pure GaAs(001) surfaces [25].

Gallium-rich surfaces appear when the (001) surface of a GaAs crystal is annealed in ultrahigh vacuum, which facilitates preferential evaporation of surface arsenic atoms [26]. The gallium-rich phase that commonly forms is the $\zeta(4 \times 2)$; figure 1(d). This surface was

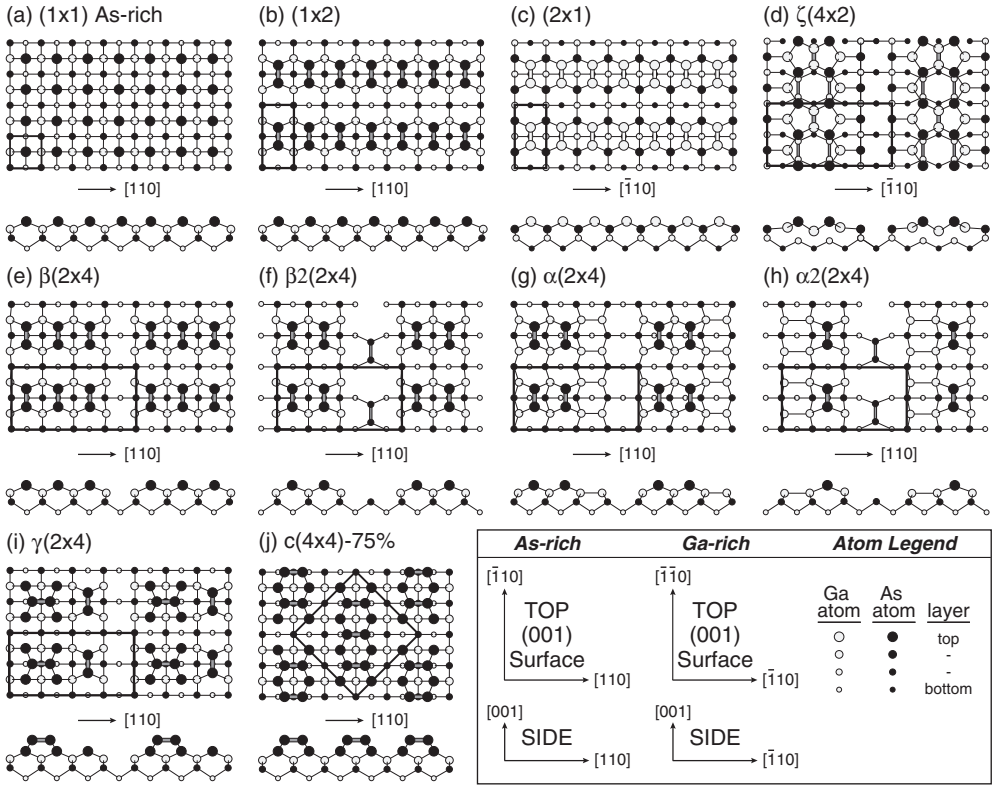

Figure 1. Suggested and observed GaAs(001) surface reconstructions. Top and side projections are shown. Unit cells are marked in black. Arsenic-rich surfaces are shown in (a), (b), and (e)–(j). The gallium-rich surfaces are shown in (c) and (d), and their lattices can be constructed from the arsenic-rich surfaces by rotating the surface 90° anticlockwise around the [001] axis, as shown in the legend box.

predicted first by DFT calculations [1] and subsequently observed by scanning tunnelling microscopy (STM) and x-ray diffraction studies [15–17] at temperatures of 800 K and above. At lower temperatures, a combination of (2×6) and (3×6) surfaces have been reported [16].

Several (2×4) arsenic-rich surface reconstructions, figures 1(e)–(i), have been identified by either theoretical calculation or experimentally using either STM or RHEED [25, 27–30]. The most reliable work to date identifies the $\beta 2(2 \times 4)$ surface [25], figure 1(f), as the dominant surface reconstruction between 780 and 820 K [14]. Variations of the $\beta 2(2 \times 4)$ reconstruction have also been reported at higher and lower temperatures [14]. Between 820 and 870 K, the surface structure deviates from the ideal $\beta 2(2 \times 4)$ structure with increased surface defect concentration (i.e., atoms are either missing or are displaced from the ideal $\beta 2(2 \times 4)$ atomic configuration), while between 750 and 850 K the surface reconstructions appear to be a combination of the $c(4 \times 4)$ and the $\beta 2(2 \times 4)$ surface structures [31, 32]. The remaining (2×4) surface reconstructions shown in figure 1 have at one time or another been suggested as low-energy structures and are included for later comparisons of DFT calculated surface free energies [14, 21, 27].

As the temperature is further lowered in the presence of an arsenic-rich atmosphere, (2×4) surface reconstructions transform into $c(4 \times 4)$ surface reconstructions [33]. The reconstruction

shown in figure 1(j) has an additional 75% coverage of arsenic dimers; however, this has been observed to vary from 25 to 100% [14]. This reconstruction appears only to occur under conditions of high arsenic vapour pressure and at temperatures between 470 and 750 K [31]. The exact structure of the additional surface dimers has recently been explored and two c(4 × 4) surface reconstruction types have been found [34]. Here, only the As–As surface is explored, so as to remain consistent with previous *ab initio* calculations [1].

2.2. *Surface free energy diagrams*

The relative stability of various compound semiconductor surface structures can be compared over a range of conditions via the calculation of equilibrium surface free energy diagrams. The thermodynamic derivation [35] and justification of the calculation method [36, 37] have been well established for systems in equilibrium. The surface free energy can be determined from the total energy, U, calculated via DFT [1] or classical potential based methods for the surface reconstructions represented in figure 1.

The surface free energies for the potentials discussed in this paper were calculated using conjugate gradient molecular statics [38], which minimizes the total energy of an ensemble of atoms. A computational slab of 1500–1700 atoms was created with two identical free surfaces, each with a surface area A. Over 25 layers of atoms separated these reconstructed surfaces and the central plane was fixed. Each layer in the computational cell measured roughly 32 Å × 32 Å (64 atoms per layer) and periodic boundary conditions were used to approximate an infinite slab in the lateral directions.

For the calculation of surface free energy, the atmosphere above the surface is assumed to serve as a reservoir for atom exchange with the GaAs(001) surface. The number of atoms is conserved during surface reactions that interchange gallium or arsenic atoms [35]. The gallium and arsenic atoms in the reservoir have a chemical potential, μ_{Ga} and μ_{As}. The surface free energy per unit area, γ, is then calculated as a function of atom configuration and composition for the computational cell [35]. The specific surface energy as $T \to 0$ K is given by

$$\gamma = \frac{1}{2\,A}\left[U^{\mathrm{tot}}_{\mathrm{slab}} - N_{\mathrm{Ga}}\,\mu_{\mathrm{Ga}} - N_{\mathrm{As}}\,\mu_{\mathrm{As}}\right], \tag{1}$$

where $2\,A$ is the surface area of the double-surfaced computational cell, $U^{\mathrm{tot}}_{\mathrm{slab}}$ is the total energy of the computational slab, N_i is the number of atoms of type i, and μ_i is the chemical potential for species i (gallium or arsenic) in the slab. The gallium and arsenic chemical potentials for the reservoir are related to the Gibbs free energy (or cohesive energy as $T \to 0$ K) per formula unit (f.u.) of the bulk GaAs crystal:

$$\mu_{\mathrm{Ga}} + \mu_{\mathrm{As}} = E^{(\mathrm{bulk})}_{\mathrm{GaAs}} = E^{(\mathrm{bulk})}_{\mathrm{Ga}} + E^{(\mathrm{bulk})}_{\mathrm{As}} + \Delta H_{\mathrm{f}}, \tag{2}$$

where $E^{(\mathrm{bulk})}_{x}$ is the cohesive energy per f.u. of either the gallium, arsenic, or GaAs systems and ΔH_{f} is the heat of formation for GaAs. The exothermic heat of formation of GaAs (ΔH_{f}) is easily defined as $\Delta H_{\mathrm{f}} = E^{(\mathrm{bulk})}_{\mathrm{GaAs}} - E^{(\mathrm{bulk})}_{\mathrm{Ga}} - E^{(\mathrm{bulk})}_{\mathrm{As}}$. Hence, the surface free energy per unit area can be re-expressed as a function of the arsenic chemical potential:

$$\gamma = \frac{1}{2\,A}\left[U^{\mathrm{tot}}_{\mathrm{slab}}\,(N_{\mathrm{Ga}}, N_{\mathrm{As}}) - N_{\mathrm{Ga}}\,E^{(\mathrm{bulk})}_{\mathrm{GaAs}} - (N_{\mathrm{As}} - N_{\mathrm{Ga}})\,\mu_{\mathrm{As}}\right]. \tag{3}$$

These reservoir chemical potentials cannot be varied indiscriminately. If the arsenic chemical potential becomes too small, then arsenic would leave the surface of the GaAs film and pure gallium would form on the surface. Likewise, if the arsenic chemical potential assumes a large negative value, then crystalline arsenic would begin to form on the surface. The bounds within which the arsenic chemical potential is controllable are [35, 37]

$$E^{(\mathrm{bulk})}_{\mathrm{As}} + \Delta H_{\mathrm{f}} < \mu_{\mathrm{As}} < E^{(\mathrm{bulk})}_{\mathrm{As}}. \tag{4}$$

This range can be simplified by subtracting the bulk arsenic free energy from both sides of the inequality in equation (4):

$$\Delta H_{\mathrm{f}} < \mu_{\mathrm{As}} - \mu_{\mathrm{As}}^{(\mathrm{bulk})} < 0, \tag{5}$$

where $E_{\mathrm{As}}^{(\mathrm{bulk})} = \mu_{\mathrm{As}}^{(\mathrm{bulk})}$, as $T \to 0$ K. The surface free energy diagram can then be plotted between zero and the GaAs heat of formation. The arsenic chemical potential range can be related to arsenic partial pressure (or arsenic concentration) assuming in ideal-gas reservoir environment [39].

The free energies (cohesive energy as $T \to 0$ K) for stable gallium, arsenic, and GaAs phases are needed to calculate the surface free energy diagram with the range of compositions (arsenic chemical potential) defined by boundaries in equation (5). The cohesive energies for lowest-energy GaAs, gallium, and arsenic phases are needed to define these boundaries in $\mu_{\mathrm{As}} - \mu_{\mathrm{As}}^{(\mathrm{bulk})}$. The lowest-energy binary GaAs phase has a zb structure [40, 41]. The corresponding terminal phases are αGa and αAs phases for elemental gallium and arsenic systems [42]. The experimental heat of formation at 298 K for GaAs was reported to be -0.736 eV/f.u. [43]. The related experimental cohesive enthalpies at 298 K for GaAs, gallium, and arsenic (ΔH_{coh}) are -6.690, -2.819, and -3.135 eV/f.u., respectively [43]. These values can be used to approximate cohesive energies per f.u. as $T \to 0$ [6].

Ab initio methods have been used to calculate the slab and bulk energies used in equation (3) to construct a GaAs(001) surface free energy diagram, figure 2(a). In figure 2(a), the solid lines correspond to surface free energy calculations by Lee *et al* [1], and the dotted lines were obtained by Ohno [44] for (1×2) and (2×1) surface reconstructions. Black lines show the lowest-energy phases; those that are represented by grey lines represent metastable phases. Under a high arsenic chemical potential (i.e., in an arsenic-rich atmosphere) the $c(4\times4)$ surface is the most stable. Over a wide intermediate range of $\mu_{\mathrm{As}} - \mu_{\mathrm{As}}^{(\mathrm{bulk})}$, the $\beta2(2 \times 4)$ surface becomes the most stable. At the lowest relative arsenic chemical potential, the gallium-rich $\zeta(4 \times 2)$ surface has the lowest surface energy. It should be noted that there is a narrow arsenic chemical potential range between the $\zeta(4 \times 2)$ and $\beta2(2 \times 4)$ stable regions where the $\alpha(2 \times 4)$ is predicted to have the lowest surface energy.

Figure 2(a) indicates that over a wide range of the arsenic chemical potential, the low-energy arsenic-rich $\beta2(2 \times 4)$ surface reconstruction is dominant. As indicated above, the $\beta(2 \times 4)$ had previously incorrectly been thought to be the most stable over this chemical range [21]. More recent DFT calculations indicate that the $\beta(2 \times 4)$ and $\beta2(2 \times 4)$ surface energies are in fact quite close. They are between 2.2 and 3.1 meV Å^{-2} of each other [1, 45]. The energy difference was attributed by Northrup and Froyen to electrostatic interactions on the polar semiconductor surface [46]. Even so, because the energy difference between $\beta(2\times4)$ and $\beta2(2 \times 4)$ surface reconstructions is small, the $\beta(2 \times 4)$ might still be seen during vapour deposition experiments [45, 47].

Figure 2(a) shows that the $\alpha2(2 \times 4)$ has the lowest energy over a very small range of compositions and is bounded by the arsenic-rich $\beta2(2 \times 4)$ and the gallium-rich $\zeta(4 \times 2)$ reconstructions [1]. The existence of this $\alpha2(2\times4)$ phase has not been validated experimentally, but a similar reconstruction may well exist locally as atmospheric conditions cause a transition between stable $\beta2(2 \times 4)$ and $\zeta(4 \times 2)$ surface reconstructions [32]. Gallium-rich $\beta(4 \times 2)$ or $\beta2(4 \times 2)$ surfaces were once thought to be stable under gallium-rich conditions [21]. These gallium-rich (4×2) reconstructions are similar to the arsenic-rich (2×4) surfaces in figure 1, except that the arsenic and gallium atom types are swapped and the surface is rotated by 90°. However, figure 2(a) indicates that these surfaces are not stable structures. Instead, the $\zeta(4\times2)$ phase with a different lattice arrangement appears to be the most stable gallium-rich surface. The understanding of these surface reconstructions has been greatly aided by DFT calculations.

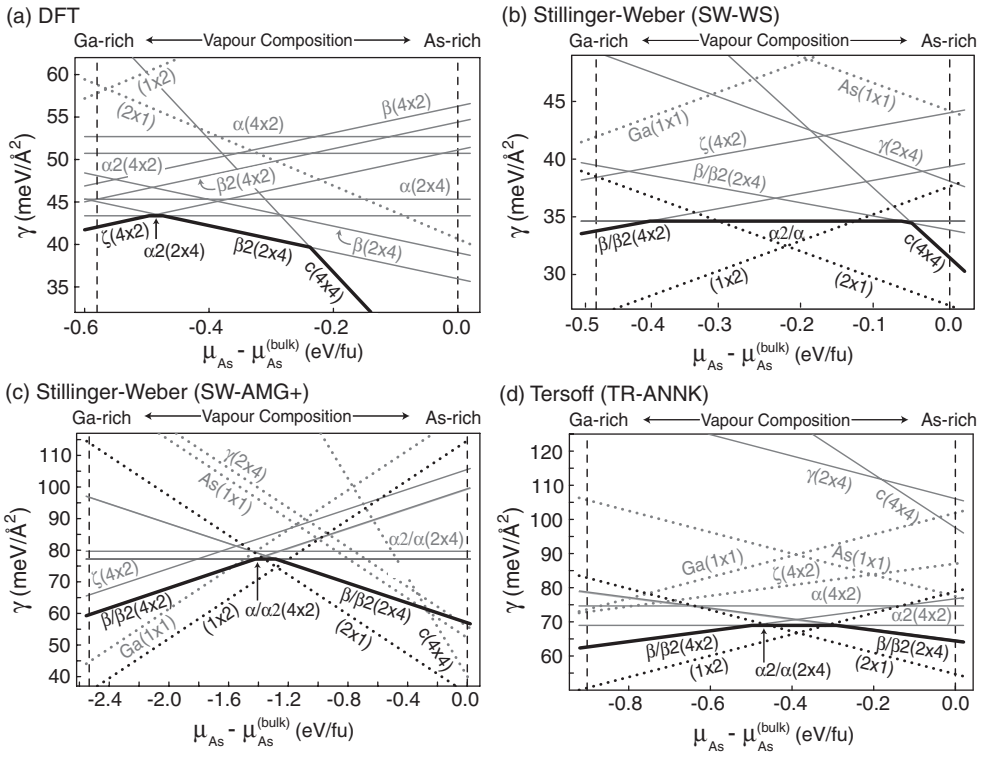

Figure 2. Surface free energy diagrams for GaAs(001) surface reconstructions, as predicted by (a) DFT [1, 44], ((b), (c)) SW, and (d) Tersoff parametrizations. The lowest-energy surface reconstructions (thick solid lines) are shown assuming surface reconstructions (· · · · · ·) are destabilized by calculations in section 6. Solid grey lines are metastable surface reconstructions. Reconstruction labels with a '/' indicate that surface free energy lines are very close or overlap; e.g., in panel (b) the $\alpha 2/\alpha$ label represents $\alpha(2 \times 4)$, $\alpha 2(2 \times 4)$, $\alpha(4 \times 2)$, and $\alpha 2(4 \times 2)$ surface reconstructions.

Although the current picture may slightly change as surface reconstructions are refined [34], a drastic change in the predicted GaAs(001) surface reconstructions is not expected.

3. Calculations using conventional potentials

Interatomic potentials provide a useful means for studying atomic structures and dynamic interactions at nanoscopic scales of length and time. By using them to calculate the total energy of a structure, potentials can then help identify the equilibrium and metastable phases of solids and the various reconstructions of their surfaces. Such potentials are developed by fitting the free parameters of physically inspired potential energy functions to material properties. Several potentials have been proposed for the GaAs system and were recently evaluated for their utility in MD simulations with free (001) surfaces [6]. The surface structure energy predictions obtained with these potentials for each of the reconstructions are shown in figures 2(b)–(d).

We began with the widely used Stillinger–Weber (SW) potential [10], which was first parametrized for GaAs by Wang and Stroud (SW-WS) [11]. A later parametrization combined

Table 1. Predicted GaAs equilibrium properties for four potential energy functions and experimental data. Heat of formation, ΔH_f, for GaAs and the cohesive energy, E_c, have units of eV/f.u.

	GaAs			Ga		As	
Potential	ΔH_f	Crys.	E_c	Crys.	E_c	Crys.	E_c
Experimental[a]	−0.74	zb	−6.69	αGa	−2.82	αAs	−3.14
SW-WS	−0.47	zb	−4.12	dc	−1.78	dc	−1.87
SW-AMG+	−2.53	zb	−5.63	dc	−1.43	fcc	−1.67
TR-ANNK	−0.92	zb	−6.71	bcc	−2.84	αAs	−2.95

[a] Reference [43].

the work of Angelo and Mills [12] and Grein *et al* [13] to construct an SW potential for GaAs (SW-AMG+). A modified multi-element Tersoff potential [9, 48] has also been used to study surface reconstructions. It was recently parametrized by Albe *et al* [7] for GaAs to model both the binary and elemental condensed phase properties. Both the potential formats and parameters used in this paper can be found in these references.

Before constructing surface free energy diagrams, the cohesive energies of the stable elemental and binary crystals were calculated for each potential. This was performed by minimizing the energy of the cubic and non-cubic crystals using the SW and Tersoff potentials [6]. The conjugate gradient method [38] was used to find the lowest-energy phase by both scaling the lattice dimensions and adjusting the internal atom positions of supercells with 100–1000 atoms. The experimental and predicted potential equilibrium structures are summarized along with cohesive energy and heat of formation data in table 1.

Experimental and potential calculations predict the GaAs zb phase to be the most stable. However, the equilibrium elemental phases and energies were not predicted with such fidelity; see a previous evaluation of properties for further detail [6]. SW potentials underestimated experimental cohesive energies for gallium and arsenic by as much as 45%. The TR-ANNK parametrization significantly improves on this performance.

A relaxed GaAs crystal was used for the surface calculations. The supercell had two identical (001) faces separated by 25–27 planes (each containing 64 atoms) to ensure the two faces did not interact. The energy of the supercell was minimized using the conjugate gradient method by scaling the volume and moving the internal atom positions. The surface area of the GaAs computational supercell was $A = 512\, r_{bulk}^2/3$, where r_{bulk} is the interatomic spacing for the equilibrium GaAs zb lattice (determined for each potential).

The calculated nearest interatomic spacings of the equilibrium bulk structures of GaAs, gallium, and arsenic, as well as the dimer spacings on the gallium-rich and arsenic-rich surfaces, are reported in table 2 together with experimental values compiled from literature. Experimental surface dimer spacings were gathered from gallium-rich $\zeta(4\times2)$ [15] and arsenic-rich $\beta2(2\times4)$ surfaces [31], while surface dimer spacings for the potentials correspond to those on the lowest-energy gallium-rich (2×1) and arsenic-rich (1×2) surfaces. Inspection of table 2 shows that the SW-WS potential predicted a uniform expansion of the bulk and surface equilibrium interatomic spacings for gallium, arsenic, and GaAs systems. Furthermore, all of the potentials predicted an expanded As–As dimer on the arsenic-rich (1×2) surface.

Relaxed surface free energies for the reconstructions shown in figure 1 were calculated using equation (3) and the data in table 1. The surface free energy was then plotted versus the relative arsenic chemical potential with boundaries defined by equation (5). These results are summarized in figure 2. Examination of the surface free energy diagrams shows that all of the potentials incorrectly predict the (2×1) gallium-rich and the (1×2) arsenic-rich surfaces

Table 2. Nearest-neighbour interatomic spacings (r) for equilibrium bulk phases and lowest-energy surface dimers. All distances are in Å. The bonding coordination, Z, is also noted for bulk phases. Surface dimer distances are taken from the uppermost surface dimer of the most stable surface reconstruction.

	Ga–As	Ga–Ga		As–As	
Potential	r_{bulk} (Z)	r_{bulk} (Z)	r_{surf}	r_{bulk} (Z)	r_{surf}
Expt.	2.443(4)[a]	2.457(1)[b]	2.445[c]	2.517(3)[b]	2.38[d]
SW-WS	2.817(4)	2.806(4)	2.898	2.863(4)	2.928
SW-AMG+	2.447(4)	2.440(4)	2.575	3.433(12)	3.193
TR-ANNK	2.448(4)	2.745(8)	2.699	2.353(3)	3.213

[a] Extrapolated to 0 K from [41].
[b] Extrapolated to 0 K from [42].
[c] Reference [15].
[d] Reference [31]. Other calculations predict 2.50–2.52 Å [49].

to be the most stable. The predicted lowest-energy (1×2) and (2×1) surfaces do not have any of the missing dimers seen experimentally in the $\beta 2(2 \times 4)$ structure or the multi-layer gallium dimerization and arsenic surface segregation seen in the $\zeta(4 \times 2)$ surfaces, figure 1.

The predicted surface energies of the $\beta(2\times4)$ and $\beta2(2\times4)$ surfaces were identical (shown as $\beta/\beta2(2 \times 4)$ in figure 2) for all of the potentials. However, experimental studies [14] and *ab initio* calculations [1] always found the $\beta2(2 \times 4)$ surface reconstruction to be more stable (by a few meV Å^{-2}). The $\beta/\beta2$ energy difference is thought to be a result of electrostatic interactions [46]. These electrostatic interactions were not directly incorporated in any of the potentials studied here, which probably makes differentiation between β and $\beta2$ surface reconstruction families impossible. A similar observation can be made for the gallium-rich $\alpha(4 \times 2)$ and $\alpha2(4 \times 2)$ surfaces. For SW-WS, the $\alpha/\alpha2(2 \times 4)$ and $\alpha/\alpha2(4 \times 2)$ were simply labelled as $\alpha/\alpha2$ in figure 2(b), because their free energies are very close. Only TR-ANNK predicts a significant energy difference between the $\alpha(4 \times 2)$ and $\alpha2(4 \times 2)$ surface structures.

During the process of finding the minimum energy for each surface supercell, the potential directs how atoms are moved on the surface. Hence, depending on the potential, the resulting structure does not always match the initial surface structures shown in figure 1. This is the case for the TR-ANNK potential's relaxation of the $\gamma(2 \times 4)$ and c(4×4). For these surfaces, the TR-ANNK parametrization predicts very weak arsenic surface dimer bonding to the arsenic-rich surface. In fact, arsenic surface dimers resided about twice as far above the surface (3.2–3.4 Å) compared to those predicted by other potentials. The TR-ANNK parameter set also fails to relax the $\zeta(4 \times 2)$ to match the experimental structure. Both SW parametrizations tend to relax the original surface reconstructions to form surface bonds with tetrahedral bond angles (109.5°).

4. Bond and dangling bond energy levels

It is well known that the surface geometries of low-index polar semiconductors are significantly influenced by the electron occupancy of bonding and dangling bond energy levels. Harrison has shown that for sp^3 hybrid orbitals, bonding and anti-bonding energy levels relevant to the GaAs surface can be estimated using the bond orbital approximation [50]. Following his approach, the surface energy levels were estimated using tight binding parameters (hopping integrals and orbital energies) calculated by the first-principles third-generation linear muffin-tin orbital

Table 3. First-principles third-generation LMTO tight binding parameters for GaAs zb, gallium dc, and arsenic dc crystals.

Parameter	Symbol	GaAs	Ga	As
Interatomic radius	r_0 (Å)	2.448	2.459	2.506
σ bond hopping integral	ssσ (eV)	−1.454	−1.632	−1.020
σ bond hopping integral	spσ (eV)[a]	1.691	1.890	1.605
σ bond hopping integral	psσ (eV)[b]	−2.147	−1.890	−1.605
σ bond hopping integral	ppσ (eV)	2.371	2.108	2.434
π bond hopping integral	ppπ (eV)	−1.012	−0.952	−0.884
s orbital energy for cation	ε_s^{Ga} (eV)	−5.070	−5.159	—
p orbital energy for cation	ε_p^{Ga} (eV)	1.377	1.429	—
s orbital energy for anion	ε_s^{As} (eV)	−10.646	—	−11.868
p orbital energy for anion	ε_p^{As} (eV)	−1.366	—	−2.434

[a] For heteropolar bonding, the arsenic s orbital overlaps the gallium p_x orbital.
[b] For heteropolar bonding, the arsenic p_x orbital overlaps the gallium s orbital.

(LMTO) method [51, 52]. These updated parameters are used to expand previous energy level calculations [53] to include Ga–Ga and As–As bonding energies. These parameters are calculated at specific interatomic separations for the GaAs zb, gallium diamond cubic (dc), and arsenic dc crystal structures and are summarized in table 3.

The atomic s and p energy levels of both gallium and arsenic combine to form sp^3 hybrids in tetrahedrally coordinated solids. The four hybrid orbitals of isolated gallium and arsenic atoms have energies of ε_h^{Ga} and ε_h^{As}, respectively. Both hybrids contribute to the total energy of the crystal when electrons occupy these orbitals. Since these energies correspond to those of the non-bonded state, they also approximate the dangling bond energies of gallium and arsenic of a free surface.

In a GaAs crystal, the hybrid orbitals overlap to form GaAs bonds with an energy ε_b^{GaAs} and GaAs anti-bonds with an energy ε_a^{GaAs}. In a solid, the GaAs bond levels spread to form a valence band and the GaAs anti-bond levels form a conduction band. Homopolar hybrid bonds also exist in arsenic and gallium dc crystals or on GaAs surfaces where As–As and Ga–Ga dimers may form. The arsenic and gallium hybrids combined to form an As–As bond with energy, ε_b^{AsAs}, and a Ga–Ga bond with energy, ε_b^{GaGa}. Five energy levels are particularly relevant to the GaAs(001) surface. They are the unbonded hybrids (ε_h^{As}, ε_h^{Ga}), bulk bonds (ε_b^{GaAs}), and surface dimers (ε_b^{AsAs}, ε_b^{GaGa}). Their energy levels are graphically represented in figure 3.

On the (001) surface, each atom has two dangling hybrid bonds on the unreconstructed (1×1) surface. Figure 3 shows that the surface energy increases when electrons occupy gallium atom hybrid dangling bonds rather than arsenic hybrid dangling bonds. Harrison showed that surfaces will reconstruct to maximize the occupancy of the arsenic dangling bonds on the surface [18]. The surface energy of (001) surfaces is also lowered when As–As and Ga–Ga dimerization occurs on arsenic-terminated and gallium-terminated planes, respectively [21].

Both relaxation and reconstruction are driven by the surface energy reductions that accompany valence electron redistribution from non-bonded high-energy levels into lower-energy bonding or arsenic dangling bond energy levels; see figure 3. Dimer formation can be addressed by the bonding terms in potentials. However, none of the current potentials address the energy penalty associated with occupation of high-energy dangling bonds or the resulting electron transfer that reduces this energy.

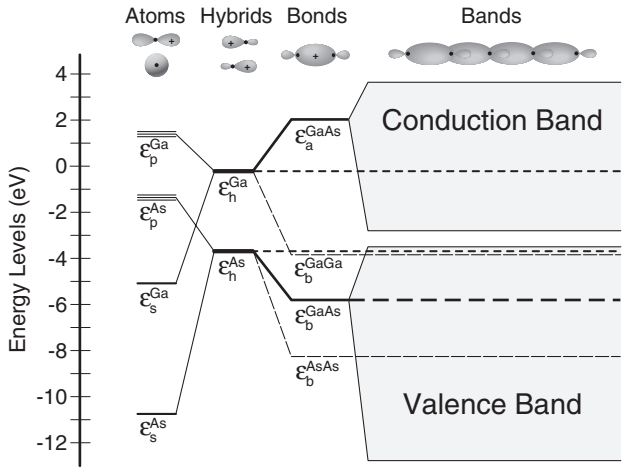

Figure 3. The energy level diagram for a GaAs surface. Gallium and arsenic unbonded (dangling bond) hybrid energies (ε_h^{Ga}, ε_h^{As}), as well as Ga–Ga (ε_b^{GaGa}), As–As (ε_b^{AsAs}), and Ga–As (ε_b^{GaAs}) bond energies are shown.

5. Electron counting models

The energy level issues identified by Harrison [18] have been summarized in the EC rule [19, 20]. This rule states that a semiconductor surface is stable only if all anion dangling bonds are fully occupied while all cation dangling bonds are empty. For a GaAs surface, this means that all surface dimer bonds, bulk covalent bonds, and arsenic (anion) dangling bonds contain two electrons while all of the gallium (cation) dangling bonds are empty. If the number of available electrons and the number of electrons needed to populate these covalent and dangling bonds are equal, then the EC rule can be satisfied. It was shown that surfaces attempt to reconstruct to achieve this surface energy reducing condition.

An EC energy penalty can be incorporated into a surface free energy calculation using classical interatomic potentials. Suppose that each atom has V_i valence electrons. If there are N atoms, the total number of valence electrons

$$V_{\text{tot}} = \sum_{i=1}^{N} V_i. \tag{6}$$

The electron occupancy in covalent and dangling bonds are parameters in the EC model. The bond between atoms i and j is required to be occupied by ξ_{ij} electrons and atom i must contain α_i electrons per dangling bond for the EC criteria to be met. Therefore, the total number of electrons required by the model is

$$V_{\text{EC}} = \tfrac{1}{2} \sum_{i=1}^{N} \sum_{j=i_1}^{i_Z} \xi_{ij} + \sum_{i=1}^{N} \alpha_i \, n_i, \tag{7}$$

where $i_1, i_2, \ldots, i_Z$ is a list of the i_Z neighbours of atom i and n_i is the total number of dangling bonds associated with atom i. The total number of dangling bonds of atom i is calculated as $n_i = \rho - i_Z$, i.e., the difference between the total number of covalent bonds formed in the bulk tetrahedral crystal, $\rho = 4$, minus the number of nearest-neighbour bonds formed around atom i, i_Z. The number of bonds, i_Z, around atom i can be counted using

$$i_Z = \sum_{j=1,\, i \neq j}^{N} \begin{cases} 1, & r_{ij} < r_{\text{cut}}^{\nu\eta} \\ 0, & r_{ij} \geqslant r_{\text{cut}}^{\nu\eta}, \end{cases} \tag{8}$$

where $r_{\text{cut}}^{\nu\eta}$ is the interatomic cut-off distance between atoms i of type ν and j of type η.

Table 4. EC parameters for each potential energy function. Cut-off distances (Å) and the energy penalty (meV per electron) parameters are reported.

Potential	w (meV/e$^-$)	$r_{\text{cut}}^{\text{GaGa}}$ (Å)	$r_{\text{cut}}^{\text{AsAs}}$ (Å)	$r_{\text{cut}}^{\text{GaAs}}$ (Å)
SW-WS	7.45	3.83	3.95	4.50
SW-AMG+	13.52	2.90	3.30	3.50
TR-ANNK	7.20	2.85	3.40	3.50

The cut-off distance is important because only covalent bonds are relevant and bonds counted outside the nearest-neighbour radius would disrupt the population of electrons.

The EC rule criterion asserts that the number of available electrons must equal the number of electrons used to populate the covalent and dangling bonds. When this difference,

$$\Delta V = V_{\text{tot}} - V_{\text{EC}}, \tag{9}$$

is greater than zero, there are excess electrons in the system that must fill higher-energy states. When it is less than zero, low-energy states remain open. In both cases the system energy is increased. This effect is estimated with a simple quadratic energy penalty, ΔE, given by

$$\Delta E = w\,\Delta V^2, \tag{10}$$

where w is an energy penalty weight. The quadratic form of equation (10) is used because it is the lowest-order non-zero term in a Taylor's series expansion of EC energy. The constant term of the Taylor expansion is irrelevant because only energy differences are considered (not absolute EC energies), and the first-order term is zero for a system in equilibrium.

In the GaAs system, the numbers of valence electrons for gallium and arsenic are $V_{\text{Ga}} = 3$ and $V_{\text{As}} = 5$. For a structure that satisfies the EC rule, the Ga dangling covalent bonds must be empty, while the arsenic dangling bonds and the remaining bonds must be full. This can be simply implemented as $\xi_{ij} = 2$, $\alpha_{\text{As}} = 2$, and $\alpha_{\text{Ga}} = 0$ in equation (7).

GaAs(001) surface reconstructions that equate V_{tot} and V_{EC} are called EC rule compliant (ECRC) surfaces. The ECRC surface reconstructions identified in this paper are: the $\beta(2\times4)$, $\beta2(2\times4)$, $\alpha(2\times4)$, $\alpha2(2\times4)$, $\beta(4\times2)$, $\beta2(4\times2)$, $\alpha(4\times2)$, $\alpha2(4\times2)$, $\gamma(2\times4)$, c(4×4) 75%, and $\zeta(4\times2)$. Surfaces that fail to comply with the EC rule (non-ECRC) include the arsenic and gallium bulk-terminated (1×1) (001) surfaces and the (2×1) and (1×2) dimer row surfaces.

6. Potential energy functions with electron counting

The addition of the EC energy to a conventional potential enables energy predictions by a potential to be modified to destabilize those that do not satisfy the EC criterion. It is important to recognize that the EC energy penalty alone does not guarantee that a potential + EC combination will produce surface free energies that reproduce experimental observations. Inaccuracies in the potential itself can still drive the surface to physically invalid predictions.

An implementation of the EC concept in conjunction with a potential requires determination of cut-off distances, $r_{\text{cut}}^{\nu\eta}$, to correctly enumerate homopolar and heteropolar bonds and identification of a realistic energy penalty parameter, w. These parameters are then inserted in equations (6)–(10) for calculating the EC energy for each surface reconstruction. The parameters for all of the potentials are summarized in table 4.

The procedure for determining the cut-off distances can be demonstrated for experimentally valid crystal structures, such as the $\zeta(4\times2)$ reconstruction. Recent

Table 5. EC adjustment to surface energy. Two surface types are shown: EC rule violating surfaces (non-ECRC) surfaces always receive an EC energy penalty; and EC rule compliant (ECRC) surfaces generally have no energy penalty but fail for specific surfaces due to potential relaxation. Note that ΔV and $\Delta\gamma$ are defined in equations (9) and (10).

			$\Delta\gamma$ (meV Å^{-2})		
Type	Surface	ΔV (e$^-$)	SW-WS	SW-AMG+	TR-ANNK
Non-ECRC	(1 × 1)-As	−192	101.3	244.0	129.8
	(1 × 1)-Ga	192	101.3	244.0	129.8
	(1 × 2)-As	−64	11.3	27.1	14.4
	(2 × 1)-Ga	64	11.3	27.1	14.4
ECRC	α2(2 × 4)	(64)[a]	0.0	27.1	0.0
	γ(2 × 4)	(64)[a]	0.0	27.1	0.0
	c(4 × 4) 75%	(64)[a]	0.0	27.1	0.0
	ζ(4 × 2)	(−256)[b]	0.0	0.0	230.7

[a] For SW-AMG+, where non-zero ΔV is caused by relaxation.
[b] For TR-ANNK, where non-zero ΔV is caused by relaxation.

experimental studies indicate that the $\zeta(4 \times 2)$ surface has second-nearest neighbours at 2.74–2.99 Å [15]. To avoid counting these second-neighbour Ga–Ga bonds, the Ga–Ga cut-off distance in equation (8) must be less than 2.74 Å. Other surfaces have different maximum distances; therefore, the cut-off distances for Ga–Ga, As–As, and Ga–As bonds were selected.

A universal choice of cut-off distances is not possible because each potential relaxes a surface differently. Satisfying EC is especially difficult when As–As or Ga–Ga surface dimers are expanded to values close to the As–As and Ga–Ga second-nearest-neighbour bond distances ($r_{2NN} = 4\,r_{1NN}/\sqrt{6}$) of the equilibrium GaAs zb structure. This is the case for the As–As bonds predicted by both the SW-AMG+ and TR-ANNK potentials. For both potentials, the As–As surface dimer bond lengths are around 3.2 Å on the (1 × 2) surface as compared to the Ga–As second-nearest-neighbour distance of 3.99 Å. The cut-offs were determined by varying the cut-off distances to find a value that satisfied ΔV in equation (9) for the greatest number of surfaces.

Values of ΔV were calculated. All ECRC surfaces should obtain $\Delta V = 0$. While the SW-WS potentials predict $\Delta V = 0$ for all of the ECRCs studied, the SW-AMG+ and TR-ANNK parametrizations give non-zero ΔV values for some of the ECRC surfaces. The non-zero ΔV values predicted by the SW-AMG+ and TR-ANNK potentials are listed in table 5. They are caused by the surface relaxation induced expansion of surface dimer length. The $\zeta(4 \times 2)$ surface predicted by TR-ANNK has a significant ΔV (and is therefore subject to a significant EC energy penalty) because both the gallium dimers are expanded by 10% and the correct $\zeta(4 \times 2)$ surface structure cannot be maintained by the potential. In addition, the $\gamma(2 \times 4)$, c(4 × 4), or α2(2 × 4) surfaces predicted by the SW-AMG+ potential have non-zero ΔV because, as was previously mentioned, the predicted surface dimers for arsenic are relatively large compared to the second-nearest-neighbour As–As interatomic spacing in the GaAs zb bulk phase; see table 2.

The EC energy penalty parameter, w, was determined from *ab initio* data for the energy difference between the β2(2 × 4) and the (1 × 2). DFT calculations predicted this energy difference to lie between 3.1 and 4.7 meV Å^{-2} (on the arsenic-rich side of the diagram) [44, 54]. Ohno's [44] value of 4.7 eV Å^{-2} was used as the energy difference between the $\beta(2\times4)$ and (1 × 2) surface reconstructions. The $\beta(2\times4)$ was chosen over the β2(2 × 4) because it was predicted to be a slightly more stable reconstruction by a fraction of an meV for the potentials studied.

The EC energy adjustment, $\Delta\gamma$, between the (1×2) and $\beta(2 \times 4)$ surfaces was then determined so that it increased the original energy difference between the two surfaces for each potential to that of a 4.7 eV Å^{-2}, as predicted by the *ab initio* calculations. With these data, the w parameters can be solved for each potential parametrization using the relation

$$\Delta\gamma = w\,(\Delta V)^2 / (2\,A)\,, \tag{11}$$

where ΔV is the difference in total number of electrons in equation (9) and $2\,A$ is the total surface area of the double-surface crystals. The results for the remaining w parameters are recorded in table 4.

A summary of the changes in surface energy, $\Delta\gamma$, imposed by EC on all structures where $V_{\rm tot} \neq V_{\rm EC}$ is reported in table 5. From these tabulated data, one can clearly see which surfaces fail to satisfy the EC criterion for each potential. These surfaces were marked in figure 2 with dashed lines, as noted in its caption. The new total surface energy for these non-ECRC surfaces can then be obtained by adding $\Delta\gamma$ to that predicted by the potentials in figure 2.

The energy difference between the gallium-rich $\beta(4\times2)$ and (2×1) surface reconstructions can also be checked. The energy difference was calculated and compared to the *ab initio* value, 13.8 meV Å^{-2} [44] (on the gallium-rich side of the diagram), for each potential. The values were determined as 3.92, 2.83, and 2.41 meV Å^{-2} for SW-WS, SW-AMG+, and TR-ANNK, respectively.

The data in table 5 and the surface free energy diagrams shown in figure 2 clearly show that non-ECRC surfaces, such as (1×2), (2×1), (1×1)-As, and (1×1)-Ga, are destabilized when electron occupancy is taken into account. By assigning an energy penalty to surfaces that fail to fill covalent bonds and arsenic dangling bonds, the potentials are now able to better predict trends in the surface free energy diagram.

The EC model presented in this paper looks at the energetics of a surface with many atoms. It does not probe mechanisms by which assembly occurs. The local phenomena such as electron transfer are not handled; thus electrons are only counted globally with no local information, i.e., this is a global model. It does not address local conditions and cannot be used to calculate force and stress. A more sophisticated EC potential will be needed to provide a molecular dynamics simulation tool for studying surface reconstructions. The next step is to develop a dynamic potential that captures the physics of EC for use in molecular dynamics simulations. A direct MD simulation of growth of the GaAs(001) surface using published potentials is currently under development.

7. Conclusions

(1) Conventional potential energy functions, such as Tersoff and Stillinger–Weber, as parametrized, all incorrectly predict the (1×2) arsenic-rich and the (2×1) gallium-rich structures as the lowest-energy surface reconstructions of a GaAs(001) surface. Missing dimer rows and other complexities seen in the $\beta2(2 \times 4)$ and $\zeta(4 \times 2)$ surface reconstructions are not captured by these potentials.

(2) The incorporation of the energy penalty associated with the electron occupancy of dangling bonds (electron counting rule) improves predictions of various surface reconstruction energies by destabilizing (1×1) bulk-terminated (001) surfaces and the dimer row ((1×2) and (2×1)) surface reconstructions for each of the potentials.

Acknowledgments

We are grateful to the Defense Advanced Research Projects Agency and the Office of Naval Research (C Schwartz and J Christodoulou, Programme Managers) for support of this work

under contract number N00014-03-C-0288. We also thank D G Pettifor, R Drautz, and S Wolf for numerous helpful technical discussions. DNM acknowledges co-funding from UK EPSRC and EURATOM.

References

[1] Lee S-H, Moritz W and Scheffler M 2000 GaAs(001) surface under conditions of low as pressure: evidence for a novel surface geometry *Phys. Rev. Lett.* **85** 3890–3

[2] Morgan C G, Kratzer P and Scheffler M 1999 Arsenic dimer dynamics during MBE growth: theoretical evidence for a novel chemisorption state of As_2 molecules on GaAs surfaces *Phys. Rev. Lett.* **82** 4886–9

[3] Itoh M 2001 Atomic-scale homoepitaxial growth simulations of reconstructed III–V surfaces *Prog. Surf. Sci.* **66** 53–153

[4] Kratzer P, Penev E and Scheffler M 2003 Understanding the growth mechanisms of GaAs and in GaAs thin films by employing first-principles calculations *Appl. Surf. Sci.* **216** 436–46

[5] Zhou X W, Wadley H N G, Johnson R A, Larson D J, Tabat N, Cerezo A, Petford-Long A K, Smith G D W, Clifton P H, Martens R L and Kelly T F 2001 Atomic scale structure of sputtered metal multilayers *Acta Mater.* **49** 4005–15

[6] Murdick D A, Zhou X W and Wadley H N G 2005 An assessment of interatomic potentials for molecular dynamics simulations of GaAs deposition. *Phys. Rev.* B submitted

[7] Albe K, Nordlund K, Nord J and Kuronen A 2002 Modeling of compound semiconductors: analytical bond-order potential for Ga, As, and GaAs *Phys. Rev.* B **66** 035205

[8] Brenner D W 1990 Empirical potential for hydrocarbons for use in simulating the chemical vapor deposition of diamond films *Phys. Rev.* B **42** 9458–71

[9] Tersoff J 1989 Modeling solid-state chemistry: interatomic potentials for multicomponent systems *Phys. Rev.* B **39** R5566–8

[10] Stillinger F H and Weber T A 1985 Computer simulation of local order in condensed phases of silicon *Phys. Rev.* B **31** 5262–71

[11] Wang Z Q and Stroud D 1990 Monte Carlo study of liquid GaAs: bulk and surface properties *Phys. Rev.* B **42** 5353–6

[12] Angelo J E and Mills M J 1995 Investigations of the misfit dislocation structure at a CdTe(001)/GaAs(001) interface using Stillinger–Weber potentials and high-resolution transmission electron microscopy *Phil. Mag.* A **72** 635–49

[13] Grein C H, Faurie J P, Bousquet V, Tournié E, Benedek R and de la Rubia T 1997 Simulations of ZnSe/GaAs heteroepitaxial growth *J. Cryst. Growth* **178** 258–67

[14] Xue Q-K, Hashizume T and Sakurai T 1999 Scanning tunneling microscopy study of GaAs(001) surfaces *Appl. Surf. Sci.* **141** 244–63

[15] Paget D, Pulci O, Sauvage M, Garreau Y, Reining L, Chiaradia P, Bechstedt F and Pinchaux R 2002 Do we understand the structure of the gallium-rich surface of GaAs(001)? Experimental and theoretical approaches *Surf. Rev. Lett.* **9** 1497–510

[16] Pristovsek M, Tsukamoto S, Ohtake A, Koguchi N, Orr B G, Schmidt W G and Bernholc J 2003 Gallium-rich reconstructions on GaAs(001) *Phys. Status Solidi* b **240** 91–8

[17] Tsukamoto S, Pristovsek M, Ohtake A, Orr B G, Bell G R, Ohno T and Koguchi N 2003 Ga-rich GaAs(001) surfaces observed by STM during high-temperature annealing in MBE *J. Cryst. Growth* **251** 46–50

[18] Harrison W A 1979 Theory of polar semiconductor surfaces *J. Vac. Sci. Technol.* **16** 1492–6

[19] Harbison J P and Farrell H H 1988 Molecular-beam epitaxial growth mechanisms on the GaAs (001) surface *J. Vac. Sci. Technol.* B **6** 733–5

[20] Pashley M D 1989 Electron counting model and its applications to island structures on molecular-beam epitaxy grown GaAs(001) and ZeSe(001) *Phys. Rev.* B **40** 10481–7

[21] Xue Q-K, Hashizume T and Sakurai T 1997 Scanning tunneling microscopy of III–V compound semiconductor (001) surfaces *Prog. Surf. Sci.* **56** 1–131

[22] Ohno H, Shen A, Matsukura F, Oiwa A, Endo A, Katsumoto S and Iye Y 1996 (Ga, Mn)As: a new diluted magnetic semiconductor based on GaAs *Appl. Phys. Lett.* **69** 363–5

[23] Tromp R M, Hamers R J and Demuth J E 1985 Si(001) dimer structure observed with scanning tunneling microscopy *Phys. Rev. Lett.* **55** 1303–6

[24] Hamers R J, Tromp R M and Demuth J E 1986 Scanning tunneling microscopy of Si(001) *Phys. Rev.* B **34** 5343–57

[25] Chadi D J 1987 Atomic structure of GaAs(100)-(2 × 1) and (2 × 4) reconstructed surfaces *J. Vac. Sci. Technol.* A **5** 834–7

[26] Kratzer P and Scheffler M 2002 Reaction-limited island nucleation in molecular beam epitaxy of compound semiconductors *Phys. Rev. Lett.* **88** 036102
[27] Farrell H H and Palmstrøn C J 1990 Reflection high energy electron diffraction characteristic absences in GaAs(100) (2 × 4)-As: a tool for determining the surface stoichiometry *J. Vac. Sci. Technol.* B **8** 903–7
[28] Yamaguchi H and Horikoshi Y 1995 Surface structure transitions on InAs and GaAs(001) surfaces *Phys. Rev.* B **51** 9836–54
[29] Frankel D J, Yu C, Harbison J P and Farrell H H 1987 High-resolution electron-energy-loss spectroscopy studies of GaAs(001) surfaces *J. Vac. Sci. Technol.* B **5** 1113–8
[30] Sauvage-Simkin M, Pinchaux R, Massies J, Calverie P, Jedrecy N, Bonnet J and Robinson I K 1989 Fractional stoichiometry of the GaAs(001) c(4 × 4) surface: an *in situ* x-ray scattering study *Phys. Rev. Lett.* **62** 563–6
[31] Ohtake A, Ozeki M, Yasuda T and Hanada T 2002 Atomic structure of the GaAs(001)-(2 × 4) surface under As flux *Phys. Rev.* B **65** 165315
[32] Takahasi M, Yoneda Y, Yamamoto N and Mizuki J 2003 Domain boundaries in the GaAs(001)-(2 × 4) surface *Phys. Rev.* B **68** 085321
[33] Biegelsen D K, Bringans R D, Northrup J E and Swartz L E 1990 Surface reconstructions of GaAs(100) observed by scanning tunneling microscopy *Phys. Rev.* B **41** 5701–6
[34] Ohtake A and Koguchi N 2003 Two types of structures for the GaAs(001)-c(4 × 4) surface *Appl. Phys. Lett.* **83** 5193–5
[35] Qian G-X, Martin R M and Chadi D J 1988 First-principles study of the atomic reconstructions and energies of Ga- and As-stabilized GaAs(100) surfaces *Phys. Rev.* B **38** 7649–63
[36] Reuter K and Scheffler M 2001 Composition, structure, and stability of RuO_2(110) as a function of oxygen pressure *Phys. Rev.* B **65** 035406
[37] Moll N, Kley A, Pehlke E and Scheffler M 1996 GaAs equilibrium crystal shape from first principles *Phys. Rev.* B **54** 8844–55
[38] Press W H 1996 *Numerical Recipes in Fortran 77: the Art of Scientific Computing* 2nd edn, vol 1 (New York: Cambridge University Press)
[39] Reuter K and Scheffler M 2002 Composition, structure, and stability of RuO_2(110) as a function of oxygen pressure *Phys. Rev.* B **65** 035406
[40] Blakemore J S 1982 Semiconducting and other major properties of gallium arsenide *J. Appl. Phys.* **53** R123–81
[41] Villars P and Calvert L D (ed) 1991 *Pearson's Handbook of Crystallographic Data for Intermetallic Phases* 2nd edn, vol 1 (Materials Park, OH: ASM International)
[42] Donohue J 1974 *The Structures of the Elements* (New York: Wiley)
[43] Lide D R (ed) 2003 *CRC Handbook of Chemistry and Physics* 83rd edn (Boca Raton, FL: CRC Press)
[44] Ohno T 1996 Theoretical study of atomic structures and dynamics on semiconductor surfaces *Thin Solid Films* **272** 331–44
[45] Sgiarovello C, Binggeli N and Baldereschi A 2004 Surface morphology and ionization potentials of polar semiconductors: the case of GaAs *Phys. Rev.* B **69** (3) 035320
[46] Northrup J E and Froyen S 1994 Structure of GaAs(001) surfaces: the role of electrostatic interactions *Phys. Rev.* B **50** R2015–8
[47] Northrup J E and Froyen S 1995 Structure and thermodynamic stability of GaAs(001) surfaces *Mater. Sci. Eng.* B **30** 81–6
[48] Brenner D W 1989 Relationship between the embedded-atom method and Tersoff potentials *Phys. Rev. Lett.* **63** 1022
[49] Schmidt W G and Bechstedt F 1996 Geometry and electronic structure of GaAs(001)(2 × 4) reconstructions *Phys. Rev.* B **54** 16742–8
[50] Harrison W A 1989 *Electronic Structure and the Properties of Solids: the Physics of the Chemical Bond* (New York: Dover)
[51] Andersen O K, Arcangeli C, Tank R W, Dasgupta T, Krier G, Jepsen O and Dasgupta I 1998 Third-generation TB-LMTO *Tight-Binding Approach to Computational Materials Science* (*MRS Symp. Proc.* vol 491) ed P E A Turchi, A Gonis and L Colombo, pp 3–34
[52] Nguyen-Manh D, Saha-Dasgupta T and Andersen O K 2003 Tight-binding model for carbon from third-generation LMTO method: a study of transferability *Bull. Mater. Sci.* **26** 27–33
[53] Harrison W A 1980 *Electronic Structure and the Properties of Solids: the Physics of the Chemical Bond* (San Francisco, CA: Freeman)
[54] Shen J H, Jiang P and Xie X D 1999 The difference between the surface reconstructions of AlAs(001) and GaAs(001) *Surf. Rev. Lett.* **6** 1167–71